JOURNAL OF MULTIFUNCTIONAL MATERIALS & PHOTOSCIENCE
11(2), December 2020, pp. 129-137

Microwave Sol-gel Based Synthesis of $Ho^{3+}/Yb^{3+}/Tm^{3+}$ tri-doped $KGd(WO_4)_2$ Phosphors and Their Upconversion Photoluminescence Properties

Chang Sung Lim
Department of Aerospace Advanced Materials & Chemical Engineering, Hanseo University, Seosan 31962, Republic of Korea
Corresponding author: cslim@hanseo.ac.kr

Abstract: Microwave sol-gel based (MSB) $Ho^{3+}/Yb^{3+}/Tm^{3+}$ tri-doped $KGd_{1-x}(WO_4)_2$ white phosphors were successfully synthesized with variations of Ho^{3+}, Yb^{3+} and Tm^{3+} (x = Ho^{3+} + Yb^{3+} + Tm^{3+}, Ho^{3+} = 0.04, 0.03, 0.02, 0.01, Yb^{3+} = 0.35, 0.40, 0.45, 0.50 and Tm^{3+} = 0.01, 0.02, 0.03, 0.04), and their upconversion (UC) photoluminescence (PL) properties were evaluated. The synthesized particles have been fairly crystallized and showed a superior microcrystalline morphology with particle sizes of 1-2 ìm. The spectroscopic properties were examined comparatively using photoluminescence emission and Raman spectroscopy. Under excitation at 980 nm, the UC doped particles revealed white emissions corresponding to the $^1G_4$ '! $^3H_6$ transitions of Tm^{3+} in the blue region, the $^5S_2$/ $^5F_4$ '! $^5I_8$ transitions of Ho^{3+} in the green region, the $^5F_5$ '! $^5I_8$ transitions of Ho^{3+} as well as the $^1G_4$ '! $^3F_4$ and $^3H_4$ '! $^3H_6$ transitions of Tm^{3+} in the red region. The pump power dependence was provided, and the individual chromacities corresponding to the equal points in the CIE diagram revealed white emissions.

Keywords: Microwave-based Synthesis, Phosphors, Upconversion, Spectroscopic, Raman

1. Introduction

Recently, the synthesis and the luminescence properties of upconversion (UC) particles have attracted considerable interest since they are considered as potentially active components in new optoelectronic devices and luminescent labels for imaging and biodetection assays, which overcome the current limitations in traditional photoluminescence (PL) materials [1-3]. Most of $MR(WO_4)_2$ (M = Li, Na, K; R = La, Gd, Y) possess the tetragonal scheelite type (ST) structure with the space group $I4_{1/a}$, and belong to the family of double tungstates compounds. It is possible for the trivalent rare earth ions in the disordered tetragonal-phase to be partially substituted by Ho^{3+} and Yb^{3+} ions, these ions are effectively doped into the crystal lattices of the tetragonal phase due to the similar radii of the trivalent rare earth ions in R^{3+}, this results in high red emitting efficiency, and superior thermal and chemical stability. In these compounds, W^{6+} is coordinated by four O^{2-} at a tetrahedral site, which makes $[WO_4]^{2-}$ relatively stable. R^{3+} and M^+ are randomly distributed over the same cationic sublattice, and they are coordinated by eight O^{2-} from near four $[WO_4]^{2-}$ with a symmetry S_4 without an inversion

center [4-6]. The $[WO_4]^{2-}$ group has strong absorption in the near ultraviolet region, so that energy transfers process from $[WO_4]^{2-}$ group to rare earth ions can easily occur, which can greatly enhance the external quantum efficiency of rare earth ions doped materials.

Multicolor and white light emissions can be generated via tri-doping system based on blue, green and red emission bands. Many lanthanide doping materials such as laser active Ho^{3+} and Tm^{3+} are employed as an activator in luminescent centers for Yb^{3+} as a sensitizer, because their unique electronic energy levels. The tri-doped Yb^{3+}, Ho^{3+} and Tm^{3+} ions can remarkably enhance the UC efficiency for the shift from infrared to visible light due to the efficiency of the energy transfer from Yb^{3+} to Ho^{3+} and Yb^{3+} to Tm^{3+}. Ho^{3+} exhibits $^5S_2/\ ^5F_4$ '! $^5I_8$ transitions in the green region, $^5F_5$ '! $^5I_8$ transitions in the red region in UC process, while Tm^{3+} shows the $^1G_4$ '! $^3H_6$ transitions in the blue region, and $^1G_4$ '! $^3F_4$ and $^3H_4$ '! $^3H_6$ transitions in the red region [7-9]. These ions are effectively doped into the crystal lattices of the tetragonal phase due to the similar radii of the trivalent rare-earth ions, these results in high red emitting efficiency, and superior thermal and chemical stability in white emitting diode.

Several processes have been developed to prepare these rare earth doped double tungstates [10-16]. A microwave sol-gel based (MSB) process provides high homogeneity, and brings a unique alternative approach for the available synthesis of high-quality PL materials [5, 6, 16]. However, the synthesis of $Ho^{3+}/Yb^{3+}/Tm^{3+}$ tri-doped $KGd(WO_4)_2$ (KGW) phosphors via the MSB route has not been reported. In this study, the double tungstate KGW phosphors with the proper doping concentrations of Ho^{3+}, Yb^{3+} and Tm^{3+} (x = Ho^{3+} + Yb^{3+} + Tm^{3+}, Ho^{3+} = 0.04, 0.03, 0.02, 0.01, Yb^{3+} = 0.35, 0.40, 0.45, 0.50 and Tm^{3+} = 0.01, 0.02, 0.03, 0.04) were successfully prepared by the MSB derived method, followed by heat treatment. The synthesized particles were characterized by X-ray diffraction (XRD) and scanning electron microscopy (SEM). The pump power dependence of the UC emission intensity and Commission Internationale de L'Eclairage (CIE) chromatic coordinates were evaluated in detail. The spectroscopic properties were examined comparatively using photoluminescence (PL) emission and Raman spectroscopy.

2. Experimental

Precise stoichiometric amounts of KNO_3 (99 %, Sigma-Aldrich, USA), $Gd(NO_3)_3$'"$6H_2O$ (99 %, Sigma-Aldrich, USA), $(NH_4)_6W_{12}O_{39}$'"xH_2O (99%, Alfa Aesar, USA), $Ho(NO_3)_3$'"$5H_2O$ (99.9%, Sigma-Aldrich, USA), $Yb(NO_3)_3$'"$5H_2O$ (99.9%, Sigma-Aldrich, USA), $Tm(NO_3)_3$'"$5H_2O$ (99.9%, Sigma-Aldrich, USA), citric acid (CA, 99.5%, Daejung Chemicals, Korea), NH_4OH (A.R.), ethylene glycol (EG, A.R.) and distilled water (DW) were used to prepare then compounds.

As the first sequence, to prepare (a) $KGd_{0.60}(WO_4)_2$:$Ho_{0.04}/Yb_{0.35}/Tm_{0.01,}$ 0.4 mol% KNO_3 and 0.067 mol% $(NH_4)_6W_{12}O_{39}$'"xH_2O were dissolved in 20 mL of EG and 80 mL of 8M NH_4OH under vigorous stirring and heating. Subsequently, 0.24 mol%

$Gd(NO_3)_3'''6H_2O$ with 0.016 mol% $Ho(NO_3)_3'''5H_2O$, 0.14 mol% $Yb(NO_3)_3'''5H_2O$ and 0.004 mol% $Tm(NO_3)_3'''5H_2O$, and DW under vigorous stirring and heating. Then, the solutions were mixed together under vigorous stirring and heating at 80-100°C. Finally, highly transparent solutions were obtained and adjusted to pH=7-8 by the addition of 8M NH_4OH. As for the doped compounds of (b) $KGd_{0.60}(WO_4)_2:Ho_{0.04}/Yb_{0.35}/Tm_{0.01,}$ 0.24 mol% $Gd(NO_3)_3'''6H_2O$, 0.016 mol% $Ho(NO_3)_3'''5H_2O$, 0.14 mol%, $Yb(NO_3)_3'''5H_2O$ and 0.004 mol% $Tm(NO_3)_3'''5H_2O$; (c) $KGd_{0.55}(WO_4)_2:Ho_{0.03}/Yb_{0.40}/Tm_{0.02,}$ 0.22 mol% $Gd(NO_3)_3'''6H_2O$, 0.012 mol% $Ho(NO_3)_3'''5H_2O$, 0.16 mol%, $Yb(NO_3)_3'''5H_2O$ and 0.008 mol% $Tm(NO_3)_3'''5H_2O$; (d) $KGd_{0.50}(WO_4)_2:Ho_{0.02}/Yb_{0.45}/Tm_{0.03,}$ 0.20 mol% $Gd(NO_3)_3'''6H_2O$, 0.008 mol% $Ho(NO_3)_3'''5H_2O$, 0.18 mol% $Yb(NO_3)_3'''5H_2O$ and 0.012 mol% $Tm(NO_3)_3'''5H_2O$; (e) $KGd_{0.45}(WO_4)_2:Ho_{0.01}/Yb_{0.50}/Tm_{0.04,}$ 0.18 mol% $Gd(NO_3)_3'''6H_2O$, 0.004 mol% $Ho(NO_3)_3'''5H_2O$, 0.20 mol%, $Yb(NO_3)_3'''5H_2O$ and 0.016 mol% $Tm(NO_3)_3'''5H_2O$. The MSB process has been previously reported in the references of [5, 6, 16].

The phase composition of the synthesized particles was identified using XRD (D/MAX 2200, Rigaku, Japan). The microstructure and surface morphology of the synthesized particles were observed using SEM (JSM-5600, JEOL, Japan). The PL spectra were recorded using a spectrophotometer (Perkin Elmer LS55, UK) at room temperature. Raman spectroscopy measurements were performed using a LabRam Aramis (Horiba Jobin-Yvon, France). The 514.5-nm line of an Ar ion laser was used as the excitation source, and the power on the samples was kept at 0.5 mW.

3. Results and Discussion

Fig. 1 shows the X-ray diffraction patterns of the synthesized (a) $KGd_{0.60}(WO_4)_2:Ho_{0.04}/Yb_{0.35}/Tm_{0.01,}$ (b) $KGd_{0.55}(WO_4)_2:Ho_{0.03}/Yb_{0.40}/Tm_{0.02,}$ (c) $KGd_{0.50}(WO_4)_2:Ho_{0.02}/Yb_{0.45}/Tm_{0.03}$, and (d) $KGd_{0.45}(WO_4)_2:Ho_{0.01}/Yb_{0.50}/Tm_{0.04,}$ particles. All of the XRD peaks could be assigned to the monoclinic-phase KGW, which was in good agreement with the crystallographic data of KGW (JCPDS 45-0555). It means that the monoclinic-phase KGW:$Ho^{3+}/Yb^{3+}/Tm^{3+}$ particles can be prepared by the MSB method. Post heat-treatment plays an important role in a well-defined crystallized morphology. To achieve a well-defined crystalline morphology, the compounds need to be heat treated at 850°C for 16 h. It is assumed that the doping amount of Ho^{3+}+Tm^{3+}/Yb^{3+} has a great effect on the crystalline cell volume of the KGW, because of the different ionic sizes. This means that the obtained samples possess a monoclinic-phase after partial substitution of Gd^{3+} by Ho^{3+}, Yb^{3+} and Tm^{3+} ions, and the ions are effectively doped into crystal lattices of the KGW phase due to the substitution of Ho^{3+} (R=1.015 Å), Yb^{3+} (R=0.985 Å) and Tm^{3+} (R=0.994 Å) ions in the Gd^{3+} (R=1.053 Å) sites [17].

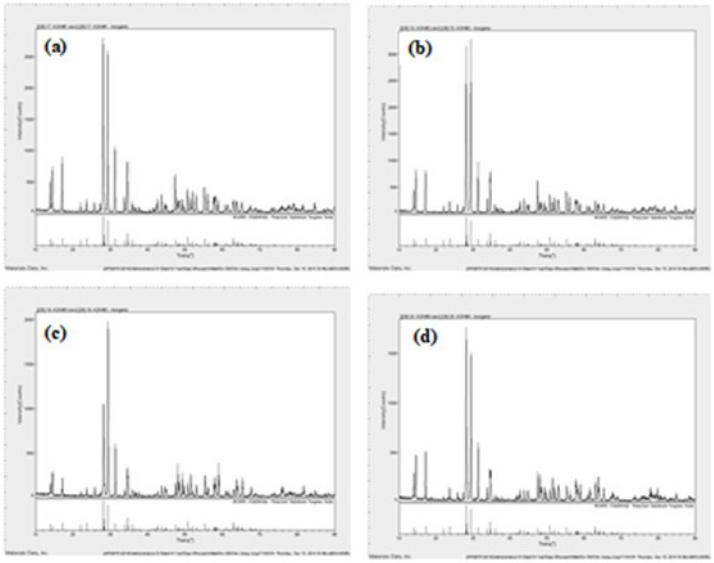

Fig. 1: XRD patterns of the synthesized (a) $KGd_{0.60}(WO_4)_2:Ho_{0.04}/Yb_{0.35}/Tm_{0.01,}$ (b) $KGd_{0.55}(WO_4)_2:Ho_{0.03}/Yb_{0.40}/Tm_{0.02,}$ (c) $KGd_{0.50}(WO_4)_2:Ho_{0.02}/Yb_{0.45}/Tm_{0.03}$, and (d) $KGd_{0.45}(WO_4)_2:Ho_{0.01}/Yb_{0.50}/Tm_{0.04,}$ particles.

Fig. 2 shows SEM images of the synthesized (a) $KGd_{0.60}(WO_4)_2:Ho_{0.04}/Yb_{0.35}/Tm_{0.01,}$ (b) $KGd_{0.55}(WO_4)_2:Ho_{0.03}/Yb_{0.40}/Tm_{0.02,}$ (c) $KGd_{0.50}(WO_4)_2:Ho_{0.02}/Yb_{0.45}/Tm_{0.03}$, and (d) $KGd_{0.45}(WO_4)_2:Ho_{0.01}/Yb_{0.50}/Tm_{0.04,}$ particles. The as-synthesized samples are very similar morphologies and no discrepancy is observed, showing superior microcrystalline morphology with particle size of 1-2 ìm. The MSB derived process of double tungstates provides unique characteristics and superior morphology for the available synthesis of UC particles.

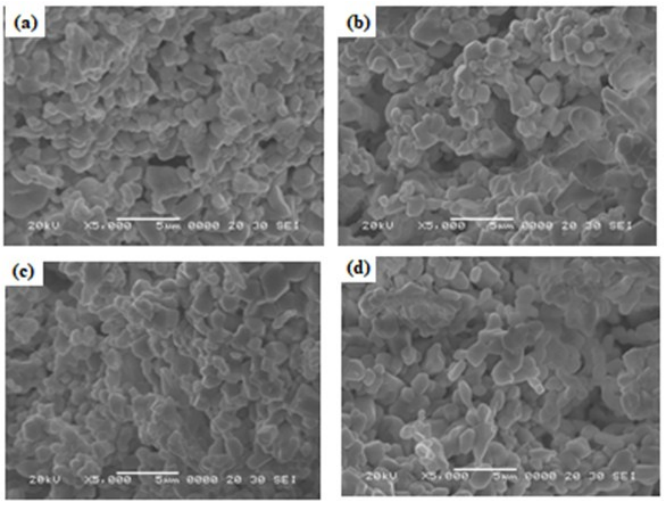

Fig. 2: SEM images of the synthesized (a) $KGd_{0.60}(WO_4)_2:Ho_{0.04}/Yb_{0.35}/Tm_{0.01,}$ (b) $KGd_{0.55}(WO_4)_2:Ho_{0.03}/Yb_{0.40}/Tm_{0.02,}$ (c) $KGd_{0.50}(WO_4)_2:Ho_{0.02}/Yb_{0.45}/Tm_{0.03}$, and (d) $KGd_{0.45}(WO_4)_2:Ho_{0.01}/Yb_{0.50}/Tm_{0.04,}$ particles.

Fig. 3 shows the UC PL emission spectra of the as-prepared (a) $KGd_{0.60}(WO_4)_2$:$Ho_{0.04}$/$Yb_{0.35}$/$Tm_{0.01,}$ (b) $KGd_{0.55}(WO_4)_2$:$Ho_{0.03}$/$Yb_{0.40}$/$Tm_{0.02,}$ (c) $KGd_{0.50}(WO_4)_2$:$Ho_{0.02}$/$Yb_{0.45}$/$Tm_{0.03}$, and (d) $KGd_{0.45}(WO_4)_2$:$Ho_{0.01}$/$Yb_{0.50}$/$Tm_{0.04,}$ particles. Under excitation at 980 nm, the doped particles exhibited white emissions based on blue, green and red emission bands, which correspond to the $^1G_4$ '! $^3H_6$ transitions of Tm^{3+} in the blue region, the $^5S_2$/ $^5F_4$ '! $^5I_8$ transitions of Ho^{3+} in the green region, the $^5F_5$ '! $^5I_8$ transitions of Ho^{3+} as well as the $^1G_4$ '! $^3F_4$ and $^3H_4$ '! $^3H_6$ transitions of Tm^{3+} in the red region [21, 22]. The UC intensity of (c) $KGd_{0.50}(WO_4)_2$:$Ho_{0.02}$/$Yb_{0.45}$/$Tm_{0.03}$ exhibits the optimal intensities of the 475-nm, 545-nm and 655-nm emission band in the blue, green and red regions, respectively. Otherwise, the UC intensity of (d) $KGd_{0.45}(WO_4)_2$:$Ho_{0.01}$/$Yb_{0.50}$/$Tm_{0.04}$ reveals the strongest 475-nm emission band in the blue region and the strongest 695-nm emission band in the red region due to higher content of Tm^{3+}. Consequently, the proper Yb^{3+}: Ho^{3+}+Tm^{3+} ratio is as high as 9:1 for the white emitting diode based on the blue, green and red emissions.

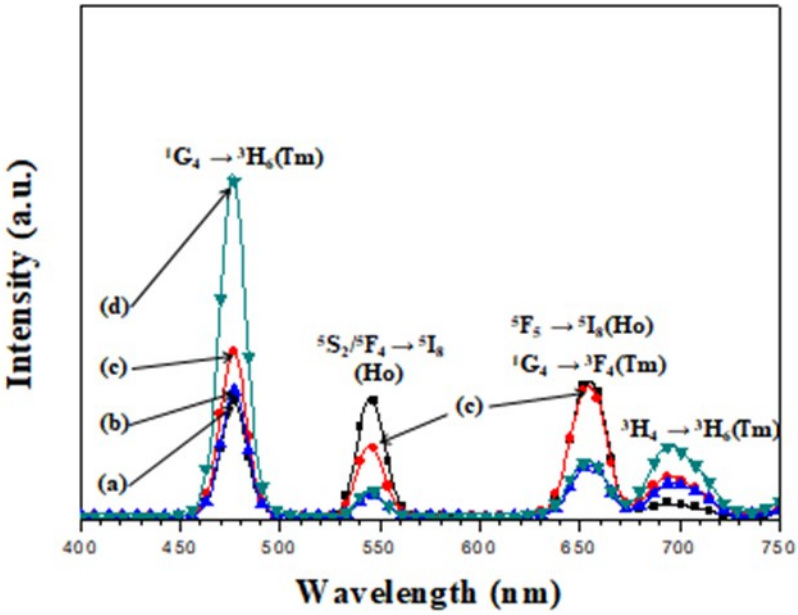

Fig. 3: UC PL emission spectra of (a) $KGd_{0.60}(WO_4)_2$:$Ho_{0.04}$/$Yb_{0.35}$/$Tm_{0.01,}$ (b) $KGd_{0.55}(WO_4)_2$:$Ho_{0.03}$/$Yb_{0.40}$/$Tm_{0.02,}$ (c) $KGd_{0.50}(WO_4)_2$:$Ho_{0.02}$/$Yb_{0.45}$/$Tm_{0.03}$, and (d) $KGd_{0.45}(WO_4)_2$:$Ho_{0.01}$/$Yb_{0.50}$/$Tm_{0.04,}$ particles excited under 980 nm at room temperature.

The logarithmic scale dependence of the UC emission intensities at 475, 545, 655 and 695 nm on the working pump power over the range of 20 to 110 mW in the $KGd_{0.50}(WO_4)_2$:$Yb_{0.02}$/$Ho_{0.45}$/$Tm_{0.03}$ sample is shown in Fig. 4. In the UC process, the UC emission intensity is proportional to the slope value n of the irradiation pumping power, where n is the number of pumped photons required to produce UC emission [18]: $I \propto P^n$ and $\ln I \propto n \ln P$, where value n is the number of the pumped photons required to excite the upper emitting state, I is the UC luminescent intensity and P is the laser pumping power. As seen from Fig. 4, the calculated slope value n = 2.70 for blue emission at 475 nm, n = 1.73 for green emission at 545 nm, and n = 1.92 and 1.90 for red emissions at

655 and 695 nm, respectively. These results show that the UC mechanism of the blue, green and red emissions can be explained by the multi-step energy transfer process in $Ho^{3+}/Yb^{3+}/Tm^{3+}$ tri-doped phosphors [7-9, 22-25].

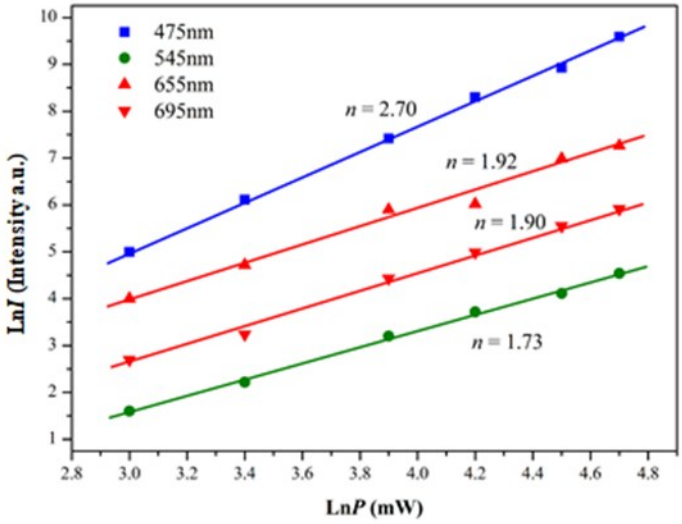

Fig. 4 : Logarithmic scale dependence of the UC emission intensity on the pump power in the range from 20 to 110 mW at 475, 545, 655 and 695 nm in the $KGd_{0.50}(WO_4)_2:Ho_{0.02}/Yb_{0.45}/Tm_{0.03}$ sample.

Fig. 5 shows (A) calculated chromaticity coordinates (x, y) values and (B) CIE chromaticity diagram for (a) $KGd_{0.60}(WO_4)_2:Ho_{0.04}/Yb_{0.35}/Tm_{0.01,}$ (b) $KGd_{0.55}(WO_4)_2:Ho_{0.03}/Yb_{0.40}/Tm_{0.02,}$ (c) $KGd_{0.50}(WO_4)_2:Ho_{0.02}/Yb_{0.45}/Tm_{0.03}$, and (d) $KGd_{0.45}(WO_4)_2:Ho_{0.01}/Yb_{0.50}/Tm_{0.04,}$ particles. The triangle depicted in Fig. 5(B) indicates standard coordinates for blue, green and red colors. The inset in Fig. 5(B) shows the chromaticity points for the samples (a), (b), (c) and (d). The chromaticity coordinates (x, y) are strongly dependent on the $Ho^{3+}/Yb^{3+}/Tm^{3+}$ concentration ratio. As indicated in Fig. 5(A), the calculated chromaticity coordinates x = 0.322 and y = 0.350 for (a) $KGd_{0.60}(WO_4)_2:Ho_{0.04}/Yb_{0.35}/Tm_{0.01,}$ x = 0.316 and y = 0.325 for (b) $KGd_{0.55}(WO_4)_2:Ho_{0.03}/Yb_{0.40}/Tm_{0.02,}$ x = 0.315 and y = 0.317 for (c) $KGd_{0.50}(WO_4)_2:Ho_{0.02}/Yb_{0.45}/Tm_{0.03}$, and x = 0.285 and y = 0.284 for (d) $KGd_{0.45}(WO_4)_2:Ho_{0.01}/Yb_{0.50}/Tm_{0.04}$ are corresponding to the standard equal energy point in CIE diagram in Fig. 6(B).

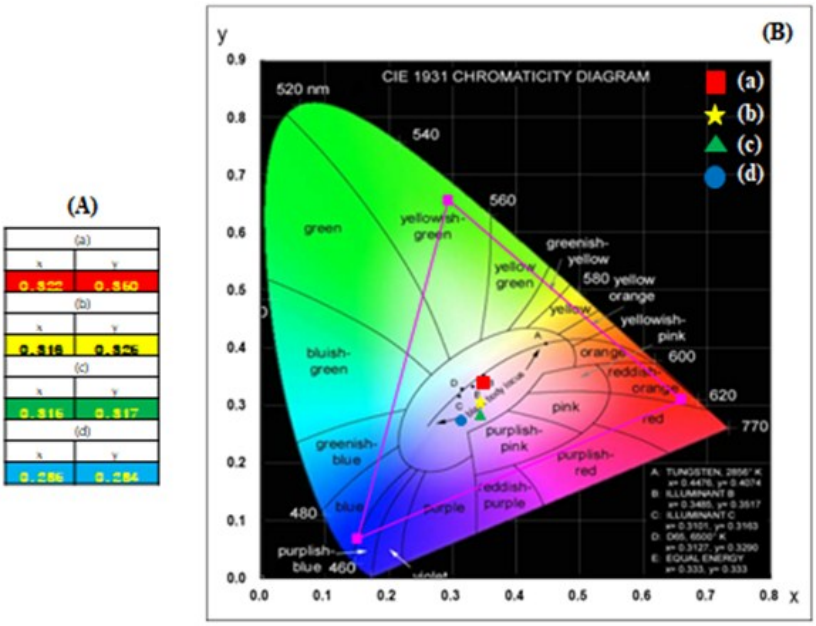

Fig. 5: (A) Calculated chromaticity coordinates (x, y) values and (B) CIE chromaticity diagram for $NaGd_{1-x}(WO_4)_2:Ho^{3+}/Yb^{3+}/Tm^{3+}$ phosphors. The inset shows the emission points for the sample synthesized (a) $KGd_{0.60}(WO_4)_2:Ho_{0.04}/Yb_{0.35}/Tm_{0.01,}$ (b) $KGd_{0.55}(WO_4)_2:Ho_{0.03}/Yb_{0.40}/Tm_{0.02,}$ (c) $KGd_{0.50}(WO_4)_2:Ho_{0.02}/Yb_{0.45}/Tm_{0.03}$, and (d) $KGd_{0.45}(WO_4)_2:Ho_{0.01}/Yb_{0.50}/Tm_{0.04,}$ particles.

Fig. 6 shows the Raman spectra of the synthesized (a) pure KGW, (b) $KGd_{0.60}(WO_4)_2:Ho_{0.04}/Yb_{0.35}/Tm_{0.01,}$ (c) $KGd_{0.55}(WO_4)_2:Ho_{0.03}/Yb_{0.40}/Tm_{0.02,}$ (d) $KGd_{0.50}(WO_4)_2:Ho_{0.02}/Yb_{0.45}/Tm_{0.03}$, and (e) $KGd_{0.45}(WO_4)_2:Ho_{0.01}/Yb_{0.50}/Tm_{0.04}$ particles excited by the 514.5-nm line of an Ar ion laser at 0.5 mW. Compared to the peaks for the (a) KGW particles, the doped compounds (b)-(e) indicate well-resolved sharp peaks for a high crystallinity state of the synthesized particles. The internal vibration mode frequencies are dependent on the lattice parameters and the strength of the partially covalent bond between the cation and molecular ionic group WO_4. The Raman spectra of the doped particles indicate the very stable and dominant peaks at higher frequencies of 688, 765, 810 and 905 cm^{-1} and at lower frequencies of 210, 235, 444 and 530 cm^{-1}. These peaks at higher and lower frequencies are attributed the strong mixing between the W-O bonds and the WO_4 stretching vibrations. The stretching vibrations of W-O bonds are observed at 688 ~ 905 cm^{-1}. For these stretching vibrations, strong mixing occurs between the W-O bonds and the WO_4. The bands at 444 and 530 cm^{-1} could be assumed to originate from vibrations of the longer W-O bonds, which are employed in the formation of the W-W bridge. The translational vibration motion of the K ions is observed around 210 ~ 235 cm^{-1}, whereas the Gd^{3+} translations were located below 180 cm^{-1} [23, 24]. The typical bands were explained in the framework of the local distortions of WO_4 tetrahedral. The high emitting efficiency of KGW:$Ho^{3+}/Yb^{3+}/Tm^{3+}$ phosphors can be considered as potentially active white emitting diodes in new optoelectronic devices.

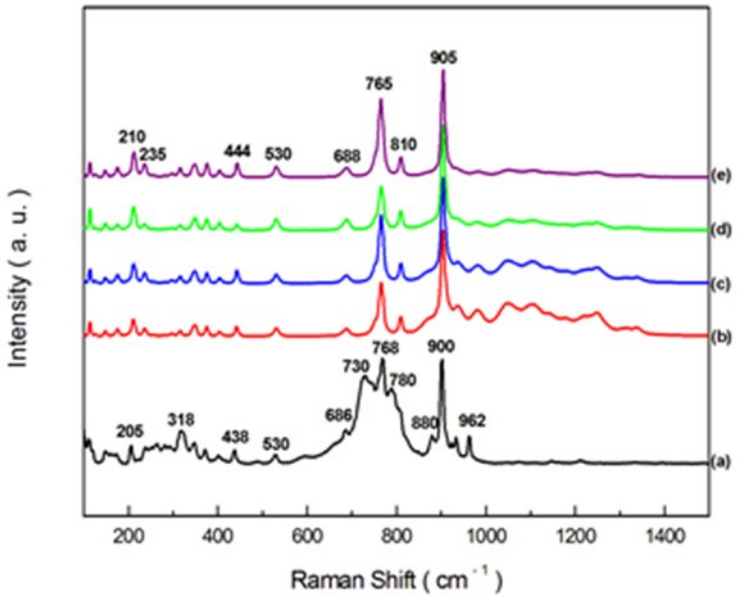

Fig. 6: Raman spectra of the synthesized (a) pure KGW, (b) $KGd_{0.60}(WO_4)_2:Ho_{0.04}/Yb_{0.35}/Tm_{0.01,}$ (c) $KGd_{0.55}(WO_4)_2:Ho_{0.03}/Yb_{0.40}/Tm_{0.02,}$ (d) $KGd_{0.50}(WO_4)_2:Ho_{0.02}/Yb_{0.45}/Tm_{0.03}$, and (e) $KGd_{0.45}(WO_4)_2:Ho_{0.01}/Yb_{0.50}/Tm_{0.04,}$ particles excited by the 514.5-nm line of an Ar ion laser at 0.5 mW.

4. Conclusions

The double tungstate KGW:$Ho^{3+}/Yb^{3+}/Tm^{3+}$ white phosphors were successfully synthesized by MSB derived method. The synthesized particles brought superior microcrystalline morphology with particle size of 1-2 ìm. Under excitation at 980 nm, the UC doped particles revealed white emissions based on blue, green and red emission bands, corresponding to the $^1G_4$ '! $^3H_6$ transitions of Tm^{3+} in the blue region, the $^5S_2/\ ^5F_4$ '! $^5I_8$ transitions of Ho^{3+} in the green region, the $^5F_5$ '! $^5I_8$ transitions of Ho^{3+} as well as the $^1G_4$ '! $^3F_4$ and $^3H_4$ '! $^3H_6$ transitions of Tm^{3+} in the red region. The proper concentration ratio Yb^{3+}:Ho^{3+}+Tm^{3+} was revealed to be 9:1 for white emitting diodes. The behavior of UC intensity is dependent on the Yb:Ho+Tm ratio and is explained in terms of the optimal number of Yb^{3+} ions at the characteristic energy transfer distance around the Ho^{3+} and Tm^{3+} ions. The calculated chromaticity coordinates were corresponding to the standard equal energy point in CIE diagram. The typical Raman bands were explained in the framework of the local distortions of WO_4 tetrahedral. The high emitting efficiency of KGW:$Ho^{3+}/Yb^{3+}/Tm^{3+}$ phosphors can be considered as potential applications of white emitting diodes in new optoelectronic devices.

Acknowledgment

This research was supported by the Basic Science Research Program through the National Research Foundation of Korea (NRF) funded by the Ministry of Science, ICT and future Planning (2018R1D1A1A09082321).

References

[1] M. Wang, G. Abbineni, A Clevenger, C. Mao, S. Xu, Nanomedicine: Nanotech. Biology, and Medicine, 7, 710 (2011).

[2] Y.J. Chen, H.M. Zhu, Y,F. Lin, X.H. Gong, Z.D. Luo, Y.D. Huang, Opt. Mat., 35, 1422 (2013).

[3] M. Lin, Y. Zho, S. Wang, M. Liu, Z. Duan, Y. Chen, F. Li, F. Xu, T. Lu, Bio. Adv., 30, 1551 (2012).

[4] L. Li, W. Zi, H. Yu, S. Gan, G. Ji, H. Zou, X. Xu, J. Lum., 143, 14 (2013).

[5] C.S. Lim, Ceramics International. 41, 2616 (2015).

[6] C.S. Lim, J. Physics and Chemistry of Solids,76, 65 (2015).

[7] J. Jin, K. Yang, J. Su, Z. Si, J. Lumin., 159, 178 (2015).

[8] Y. Xu, Y. Wang, L. Xing, X. Tan, 54, 50 (2013).

[9] D. Li, Y. Wang, X. Zhang, G.Shi, G. Liu, Y. Song, J. Alloys Compd., 550, 509 (2013).

[10] X. Liu, W. Xiang, F. Chen, W. Zhang, Z. Hu, Mater. Res. Bull., 47, 3417 (2012).

[11] X. Liu, W. Xiang, F. Chen, Z. Hu, W. Zhang, Mater. Res. Bull., 48, 281 (2013).

[12] N. Xue, X. Fan, Z. Wang, M. Wang, Mater. Lett., 61, 1576 (2007).

[13] S. Huang, D. Wang, Y. Wang, L. Wang, X. Zhang, P. Yang, J. Alloys Compd., 529, 140 (2012).

[14] J. Feng, J. Xu, Z. Zhu, Y. Wang, Z. You, J. Li, H. Wang, C. Tu, J. Alloys Compd., 566, 229 (2013).

[15] F. Song, L. Han, H. Tan, J. Su, J. Yang, J. Tian, G. Zhang, Z. Cheng, H. Chen, Opt. Comm., 259, 179 (2006).

[16] C.S. Lim, Mater. Res. Bull., 47, 4220 (2012).

[17] R. D. Shannon, Acta Cryst., A32, 751 (1976).

[18] H. Guo, N. Dong, M. Yin, W. Zhang, L. Lou, S. Xia, J. Phys. Chem. B, 108, 19205 (2004).

[19] Y. Xu, Y. Wang, L. Shi, L. Xing, X. Tan, Opt. Laser Tech., 54, 50 (2013).

[20] X. Li, Q. Nie, S. Dai, T. Xu, L. Lu, X. Zhang, J. Alloys Compd., 454, 510 (2008).

[21] L.G.A. Carvalho, L.A. Rocha, J.M.M. Buarque, R.R. Goncalves, C.S. Nascimento Jr., M.A. Schavon, S.J.L. Ribeiro, J.L. Ferrari, J. Lumin., 159, 223 (2015).

[22] H. Gong, D. Yqang, X. Zhao, E.Y.B. Pun, H. Lim, Opt. Mater., 32, 554 (2010).

[23] V.V. Atuchin, O.D. Chimitova, T.A. Gavrilova, M.S. Molokeev, Sung-Jin Kim, N.V. Surovtsev, B.G. Bazarov, J. Crys. Growth, 318, 683 (2011).

[24] V.V. Atuchin, O.D. Chimitova, S.V. Adichtchev, J.G. Bazarov, T.A. Gavrilova, M.S. Molokeev, N.V. Surovtsev, Zh.G. Bazarova, Mater. Lett., 106. 26 (2013).